Spectral Proper Orthogonal Decomposition Analysis of Shock-Wave/Boundary-Layer Interactions

Stephanie M. Cottier[1] and Christopher S. Combs[2]
The University of Texas at San Antonio, San Antonio, TX, 78249

Shock-wave/boundary-layer interactions (SWBLIs) are a major concern in the development of high-speed aircraft. SWBLIs generate low-frequency unsteadiness in many aerodynamic applications and often lead to flow separation and an increased likelihood of scramjet engine unstart. Existing research on SWBLIs has focused primarily on either fully laminar or fully turbulent interaction boundary layers and utilizes frequently employed visualization methods such as planar laser scattering (PLS), particle image velocimetry (PIV), and Schlieren imaging. Despite the breadth of research conducted, a definitive driving mechanism of this unsteadiness is still yet to be determined. Building upon previous work, the current research focuses on analyzing high-speed Schlieren images of cylinder-induced transitional SWBLIs (XSWBLIs) in a Mach 5 wind tunnel using spectral proper orthogonal decomposition (SPOD).The appeal of using SPOD analysis over similar methods is that SPOD produces modes that are coherent in both space and time. Using a set of 5,000 Schlieren images previously collected at the Center for Aeromechanics Research Wind Tunnel Laboratory at The University of Texas at Austin, an SPOD analysis of the interaction structure was conducted for the representative XSWBLI test case. These results serve mainly as a proof of concept for the practicality of SPOD analysis of XSWBLIs but also shed light on the underlying physics of the interaction. Upon studying the resulting SPOD modes it was observed that lower order modes develop coherent physical structures in the form of a leading edge shock, Upstream Influence (*UI*), inviscid shock, forward lambda-shock (λ_1),downstream closure shock (λ_2), and the flow separation beneath the lambda-shock structure. These features become less prominentas frequency and mode number increase. Plots of the modal energies of selected modes as a function of Strouhal number show fluctuations in the modal energies for Mode 1. These fluctuations indicate unsteadiness generated by the XSWBLI. The largest of these fluctuations occurs between *St* = 0.01 – 0.03 and further analysis produced promising SPOD results. Optimizing certain parameters within the SPOD algorithm should yield more germane modal structures in future analysis.

Nomenclature

SPOD	=	Spectral Proper Orthogonal Decomposition
POD	=	Proper Orthogonal Decomposition
DMD	=	Dynamic Mode Decomposition
FFT	=	Fast Fourier transform
DFT	=	Discrete Fourier transforms
$\boldsymbol{Q}$	=	Snapshot data Matrix
$\boldsymbol{q}_k$	=	Snapshot data vector
t_k	=	Time
M	=	Number of snapshots in data set
N_b	=	Number of data blocks
N_f	=	Number of snapshots in a data block
$\boldsymbol{Q}^{(n)}$	=	Snapshot data block
$\boldsymbol{q}_k^{(n)}$	=	Snapshot data vector representing the *k*-th entry in the *n*-th block
$\widehat{\boldsymbol{Q}}^{(\boldsymbol{n})}$	=	Discrete Fourier transform of the *n*-th snapshot data block
$\widehat{\boldsymbol{q}}_k^{(n)}$	=	Fourier Component at the *k*-th discrete frequency in the *n*-th block

[1]Masters of Science Candidate, Department of Mechanical Engineering, AIAA Student Member.
[2]Dee Howard Endowed Assistant Professor, Department of Mechanical Engineering, Member AIAA.

f = Frequency
$\widehat{\boldsymbol{Q}}_{f_k}$ = Fourier data matrix at frequency f_k
w_j = Scalar weights
$\boldsymbol{S}_{f_k}$ = Cross-spectral density tensor at frequency f_k
$\widehat{\boldsymbol{Q}}^*_{f_k}$ = Hermitian–transpose of the Fourier data matrix
d = Cylinder diameter
U = Freestream velocity
UI = Upstream influence shock
λ_1 = Forward shock
λ_2 = Downstream closure (rearward) shock
St = Strouhal number
λ = Modal energy
i = Mode number

I. Introduction

With the increased interest in high-speed aircraft over recent decades, the importance of understanding shock-wave/boundary-layer interactions (SWBLIs) has become more prominent. SWBLIs generate low-frequency unsteadiness in many aerodynamicapplications and often lead to flow separation and an increased possibility of engineunstart in scramjet engines.[1,2] The majority of existing research on SWBLIs has been conducted in either fully laminar or fully turbulent boundary layers.[3] Despite the breadth of research conducted, a definitive driving mechanism of this unsteadiness is still yet to be determined, though there has been some evidence suggesting that strong interactions with larger separation bubbles are the result of oscillations of a downstream instability while weaker interactions with smaller separations are driven by fluctuations in the incoming boundary layer.[4] Clemens and Narayanaswamy[4] reviewed research from the past few decades to study the source of low-frequency unsteadiness of shock-wave/turbulent boundary-layer interactions. Their scope focused on interactions caused by compression ramp, reflected shock, and cylinder on flat plate geometries. From the results of their review, the authors argue that both the upstream boundary layer and the downstream instability work together on all interactions. However, they note that the degree of influence of the upstream boundary layer appears to decrease as the separation bubble increases.

While turbulent and laminar interactions have been the focus of the majority of previous studies, research on shock-wave/transitional boundary-layer interactions (XSWBLI) is an emerging area focusing on the internal mechanisms of these interactions.[1,4,5,6] Previous research conducted by Murphree et al.[5,7] examined SWBLIs generated by a cylinder mounted on a flat plate in a Mach 5 flow. Planar laser scattering (PLS) and particle image velocimetry (PIV) were used to visualize the flow structure as the cylinder was moved farther from the leading edge of the plate. Analysis of the PLS visualizations concluded that in transitional boundary layers, the separated flow region shows greater variations in shape and scale than fully turbulent boundary layers. In addition, the transitional boundary layer resulted in two types of separation shock, which were not apparent in fully turbulent interactions. These findings were confirmed by the PIV measurements. More recently, Combs et al.[1,6] studied cylinder-induced SWBLIs in transitional and fully turbulent boundary layers in a Mach 1.78 flow. High-speed Schlieren images were used to track the positions of the upstream influence shock, forward lambda shock, and trailing lambda shock in a time-resolved manner. Spectral analysis of the Schlieren images revealed energy peaks in the separated flow region. This suggests that the unsteadiness in the transitional interactions is heavily influenced by instability in the separated flow region.

Building upon previous work by Combs et al., Murphree et al., and Towne et al., the current research focuses on analyzing high-speed Schlieren images of cylinder-induced SWBLIs in a Mach 5 wind tunnel using spectral proper orthogonal decomposition (SPOD).[1,6,8,10] The advantage of using SPOD analysis over similar methods like dynamic mode decomposition (DMD) or proper orthogonal decomposition (POD), is that SPOD is coherent in both space and time. For this reason, SPOD may be a better option for identifying physically meaningful coherent structures in fluid flows and investigating the driving mechanisms behind SWBLI unsteadiness.[8]

II. Theory

POD is a frequently employed analysis tool used to reduce data into modes by decomposing what is known as the spatial correlation tensor.[8] This process produces spatially orthogonal modes that lose all concept of sequential ordering and therefore have random time dependence. Since temporal correlation is an essential feature of physical

coherent structures, this means that POD modes are not constructed to represent flow structures that evolve coherently. Analternative to POD is DMD, which identifies coherent structures from flow dynamics. But where POD results in spatially orthogonal modes with random time dependence, DMD does the opposite, resulting in temporally orthogonal modes that are spatially non-orthogonal.[8]

SPOD attempts to bridge the gap between POD and DMD. SPOD refers to the frequency domain form of POD. Like POD, SPOD refines data into modes, but does so by decomposing what is known as the cross-spectral density tensor. Where POD results in modes that are only spatially coherent,SPOD yields modes that evolve coherently in space and time. Thetime dependence is retained due to the use of a fast Fourier transform (FFT) to calculate row-wise discrete Fourier transforms (DFT) from smaller blocks of data.[8]

SPOD analysis uses an algorithm known as Welch's method to refine the raw data.[9] A schematic depiction of this is shown in Figure 1.

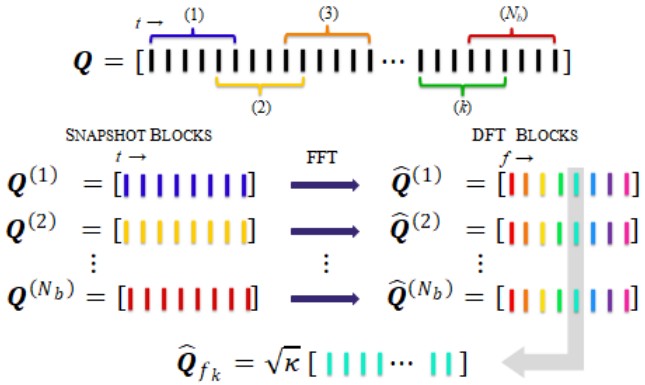

Figure 1. Schematic depiction of Welch's method for estimating SPOD modes (Adapted from Ref. 8).

First, the data are compiled into a matrix:

$$\boldsymbol{Q} = [\boldsymbol{q}_1,\ \boldsymbol{q}_2, \dots,\ \boldsymbol{q}_k, \dots,\ \boldsymbol{q}_M] \in \mathbb{R}^{N \times M} \tag{1}$$

where $\boldsymbol{q}_k$ is a vector, or snapshot, representing the instantaneous state of $\boldsymbol{q}(\boldsymbol{x}, t)$at time$t_k$ and M designates the total number of snapshots. The data matrix is then broken down into smaller sets called blocks. There are N_b number of blocks and N_f is the number of snapshots in each block. Sometimes, the blocks overlap and share snapshots. Blocks can be depicted mathematically by the equation

$$\boldsymbol{Q}^{(n)} = \left[\boldsymbol{q}_1^{(n)},\ \boldsymbol{q}_2^{(n)}, \dots,\ \boldsymbol{q}_k^{(n)}, \dots,\ \boldsymbol{q}_{N_f}^{(n)}\right] \in \mathbb{R}^{N \times N_f}. \tag{2}$$

Here,$\boldsymbol{q}_k^{(n)}$ represents the k-th entry in the n-th block. Next, the DFT for each block is computed using an FFT

$$\widehat{\boldsymbol{Q}}^{(\boldsymbol{n})} = FFT\left(\boldsymbol{Q}^{(\boldsymbol{n})}\right) = [\widehat{\boldsymbol{q}}_1^{(n)}, \widehat{\boldsymbol{q}}_2^{(n)}, \dots, \widehat{\boldsymbol{q}}_k^{(n)}, \dots, \widehat{\boldsymbol{q}}_{N_f}^{(n)}] \tag{3}$$

where $\widehat{\boldsymbol{q}}_k^{(n)}$ is the Fourier component at the k-th discrete frequency, f_k, in the n-th block. A new data matrix is then created by compiling the Fourier components at frequency f_k from each block into the equation

$$\widehat{\boldsymbol{Q}}_{f_k} = \sqrt{\kappa}\,[\widehat{\boldsymbol{q}}_k^{(1)}, \widehat{\boldsymbol{q}}_k^{(2)}, \dots, \widehat{\boldsymbol{q}}_k^{(N_b)}] \in \mathbb{R}^{N \times N_b} \tag{4}$$

where $\kappa = \Delta t / sN_b$ and $s = \sum_{j=1}^{N_f} w_j^2$. The scalar weights, w_j, are nodal values of a window function used to mitigate complications caused by non-periodicity of the data in each block. The data matrix $\widehat{\boldsymbol{Q}}_{f_k}$ is then used to estimate the cross-spectral density tensor at frequency f_k as follows

$$\boldsymbol{S}_{f_k} = \widehat{\boldsymbol{Q}}_{f_k} \widehat{\boldsymbol{Q}}_{f_k}^{*} \tag{5}$$

where $\widehat{\boldsymbol{Q}}_{f_k}^{*}$ designates the Hermitian–transpose of the tensor. As the number of blocks, N_b, and the number of snapshots in each block, N_f, increase simultaneously, this estimate converges. This reduces an infinite dimensional SPOD eigenvalue problem to an $N \times N$ matrix eigenvalue problem. From there, the cross-spectral density tensor is broken up using spectral (eigenvalue) decomposition and used to calculate the SPOD modes.

SPOD modes are actually optimally averaged DMD modes, each of which oscillate at a single frequency. Unlike DMD modes however, SPOD modes represent space-time flow phenomena. The culmination of this being structures that evolve coherently in space and time. Because they divide flow data at different time scales while remaining spatially orthogonal, SPOD modes have been shown to be more effective in the analysis of unsteady flow phenomena than POD or DMD modes.[8]

III. Experimental Program

A. Experimental Facility

The experiments were conducted in the Mach 5 blow-down wind tunnel located at the Center for Aeromechanics Research on the J. J. Pickle Research Campus at The University of Texas at Austin. The facility utilizes a bottle field of four tanks with a combined storage volume of 4 m^3 and a maximum pressure of 17.2 MPa. The stagnation pressure and temperature are 2.5 MPa and 350K. The constant-area test section measures 686 mm long by 178 mm high and 152 mm wide.[10]

B. Model Geometries

The SWBLIs being examined for this experiment were generated by a circular cylinder on a flat plate. The plate measures 254 mm long and has 12˚ leading and trailing edges and is mounted to the wind tunnel sidewalls. A 9.5 mm diameter cylinder was mounted to the plate via a compression screw-jack and can be translated in the streamwise direction along the plate to generate SWBLI in different regions of the developing boundary layer. For this experiment, the cylinder was positioned approximately $10d$ downstream of the leading edge to generate XSWBLI.[10]

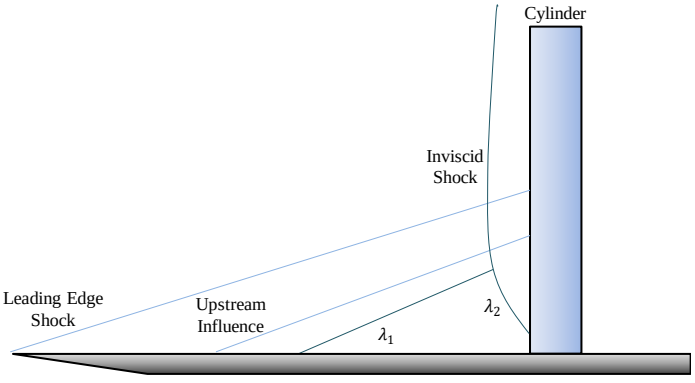

Figure 2. Schematic of Cylinder/Flat Plate model, where λ_1 is the forward shock and λ_2 is the downstream closure shock (Adapted from Ref. 10).

C. Experimental Systems

The Schlieren system was configured in a Z-type setup using 305 mm diameter mirrors. A high-powered, pulsed light-emitting diode served as the light source and a razor blade as the knife edge. A Photron FASTCAM Mini UX100 high-speed camera was used to capture the images at a frame rate of 80 kHz.[1]

IV. Results

A set of 5000 Schlieren images were used to conduct the SPOD analysis. The results of the data set serve mainly as a proof of concept for the practicality of SPOD analysis of SWBLIs. The SPOD modes were calculated using Welch's method outlined above. Using MATLAB, data were separated into 38 blocks, each containing 256 snapshots. Data blocks were then used to calculate temporal DFT blocks, and ultimately, the SPOD modes. Resulting frequencies range from 0.0 kHz to 38.7 kHz. The eigenvalues (λ) of the SPOD modes represent their modal energies. The SPOD algorithm arranges modes by descending energy levels, i.e. Mode 1 will have the highest energy and the last mode, Mode 38, will have the lowest energy.

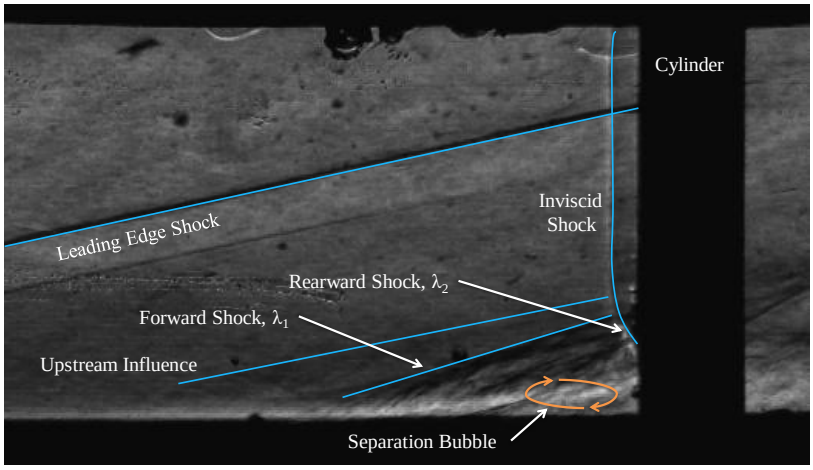

Figure 3. Schlieren image of 9.5 mm diameter cylinder on a flat plate in Mach 5 wind tunnel.

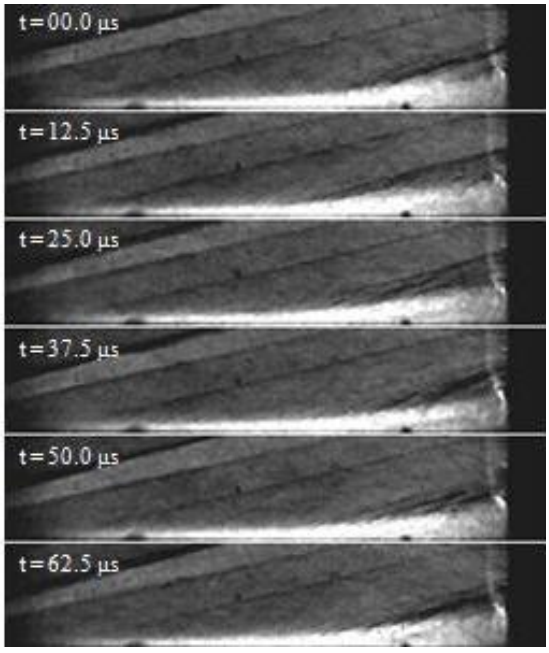

Figure 4. Time sequence of shock motion, where time is in micro-seconds (*µs*).

Figure 3 shows a representative Schlieren image from the XSWBLI experiment. Key features have been highlighted for clarity, including the upstream influence shock (*UI*), the forward shock (λ_1), the downstream closure shock (λ_2), and the separation bubble underneath the lambda shock structure.The transitional boundary layer and leading edge shock are also clearly visible. A time montage of Schlieren images in Figure 4 provides a snapshot of the motion of the shock structures from the data set. The upstream influence shock present in the data set is a feature shown to form in XSWBLIs and dissipate as the boundary layer becomes turbulent.[1] Fluctuations can be seen in the position and intensity of the forward shock and the separation bubble as well as the thickness and turbulence of the boundary layer. Examining the figure, these features move together as a system: as the separation bubble grows the boundary layer also grows and the relative position of the forward shock increases. Conversely, as the separation bubble decreases, so does the boundary layer thickness and the relative position of the forward shock. An average of the shock motion from the first 100 images of the data set is compiled in Figure 5. This provides an estimation of the locations where the *UI*, λ_1, and λ_2 are likely to form and the thickness of the boundary layer and the separation bubble.

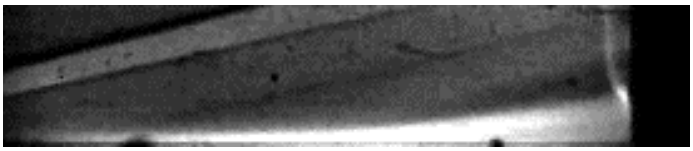

Figure 5. Average of First 100 Schlieren Images

Two-dimensional reconstructions of select modes are plotted for several frequencies in Figure 11 -Figure 11. These modes were chosen to compare the high modal energy of the lower modes to the higher order, lower energy modes. The plots are divided into sets by frequency, including 1 kHz, 2 kHz, 5 kHz, 10 kHz, 20 kHz, and 38.7 kHz (the highest mode frequency in the present analysis). The lower modes develop coherent physical structures in the form of a leading edge shock, upstream influence, inviscid shock, forward shock, and the downstream closure shock as well as the flow separation beneath them. These features become less coherent as mode numbers increase due to the amount of small-scale turbulence being captured in the lower energy modes. In general, there is also a loss of coherence as frequency increases. Comparing Figure 11 with Figure 6Figure 10, it is clear that the 38.7 kHz modes have the least coherent structures and the most small-scale turbulence. Hence, SWBLI generated unsteadiness can best be studied by analyzing high-energy modes at frequencies less than 2 kHz, or a Strouhal number (*St*) of 0.03 or less. These numbers are in agreement with results from earlier analysis which indicate unsteady shock breathing at low-frequencies[11-18], corresponding with Strouhal numbers between 0.02 – 0.1.[1,3,4,11] Strouhal number is a dimensionless parameter calculated by $St = {fd}/{U}$, where f is frequency, d is cylinder diameter, and U is the freestream velocity.

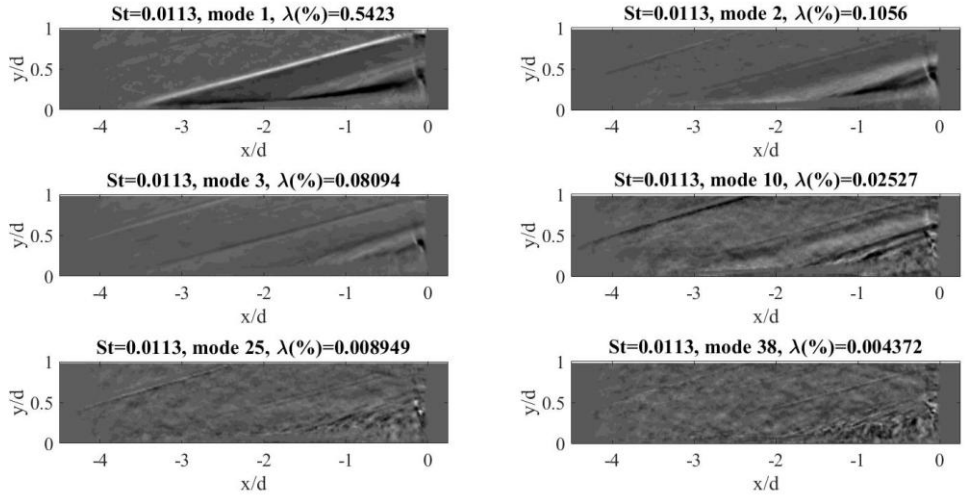

Figure 6. 2-D Plots of Selected Modes at 1 kHz

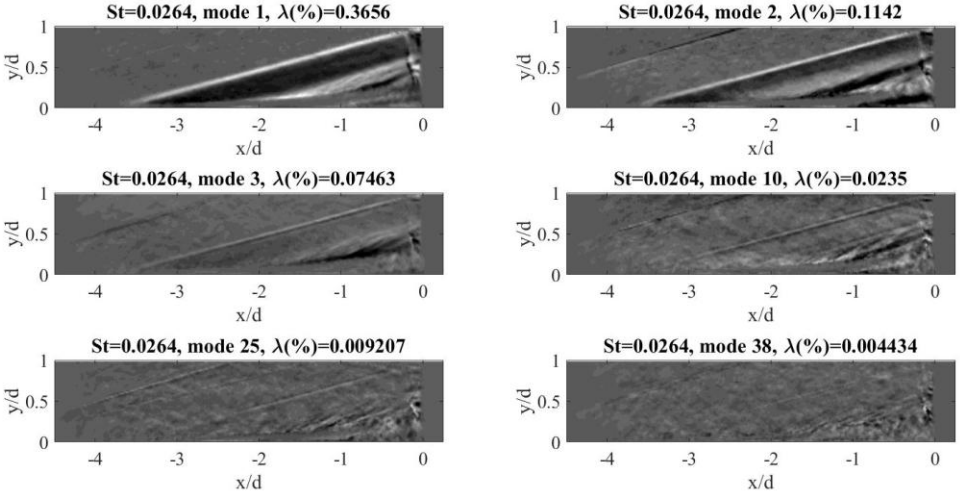

Figure 7. 2-D Plots of Selected Modes at 2 kHz

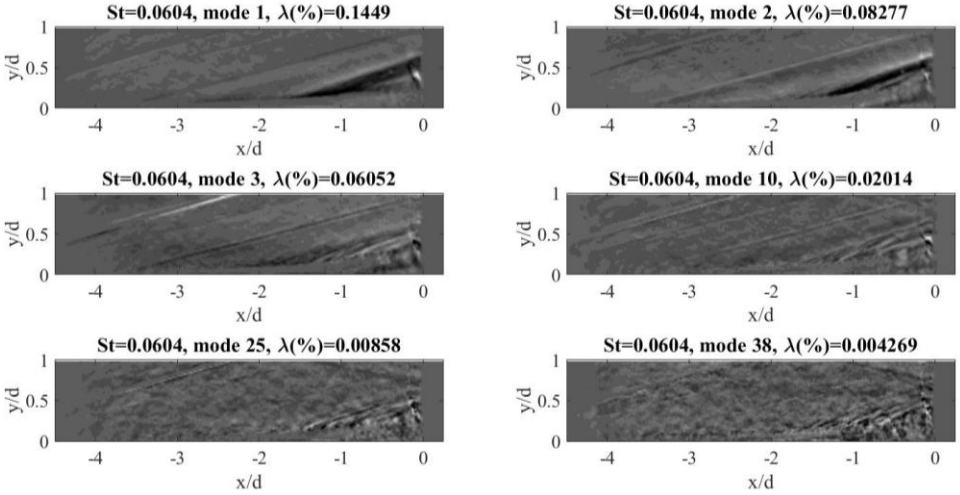

Figure 8. 2-D Plots of Selected Modes at 5 kHz

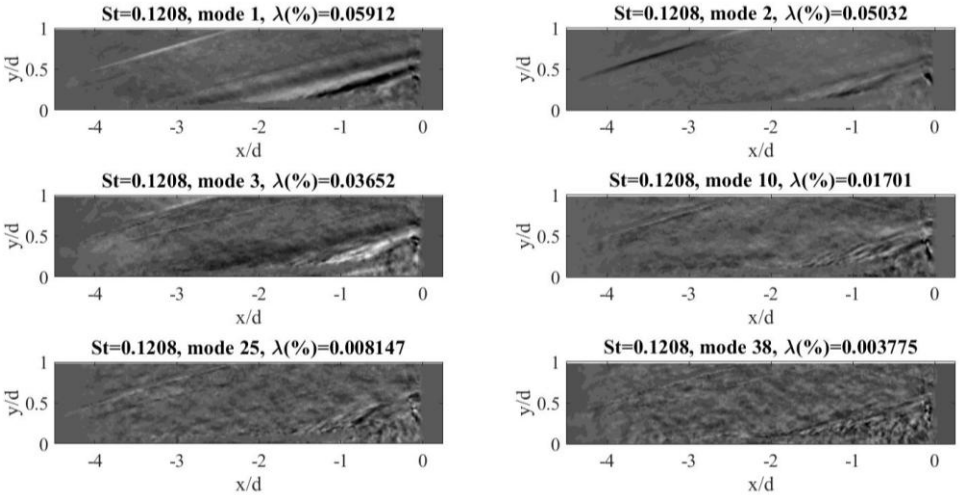

Figure 9. 2-D Plots of Selected Modes at 10 kHz

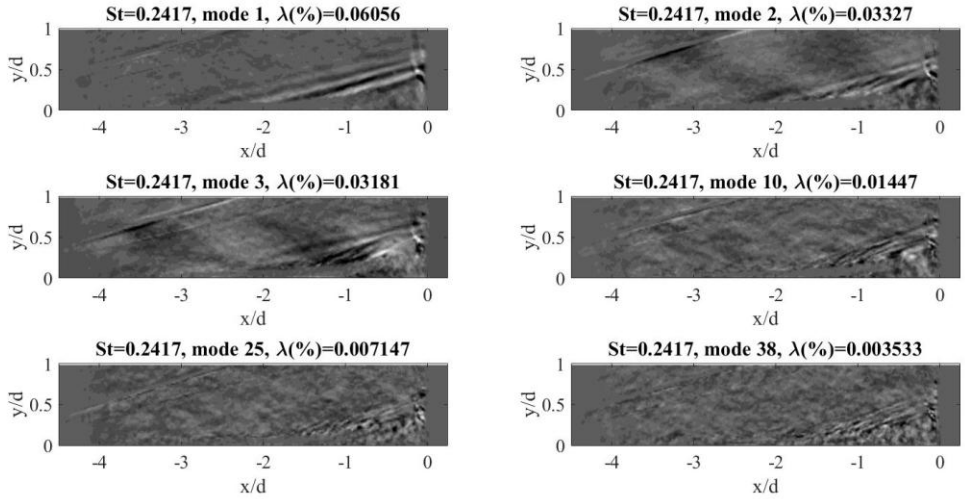

Figure 10. 2-D Plots of Selected Modes at 20 kHz

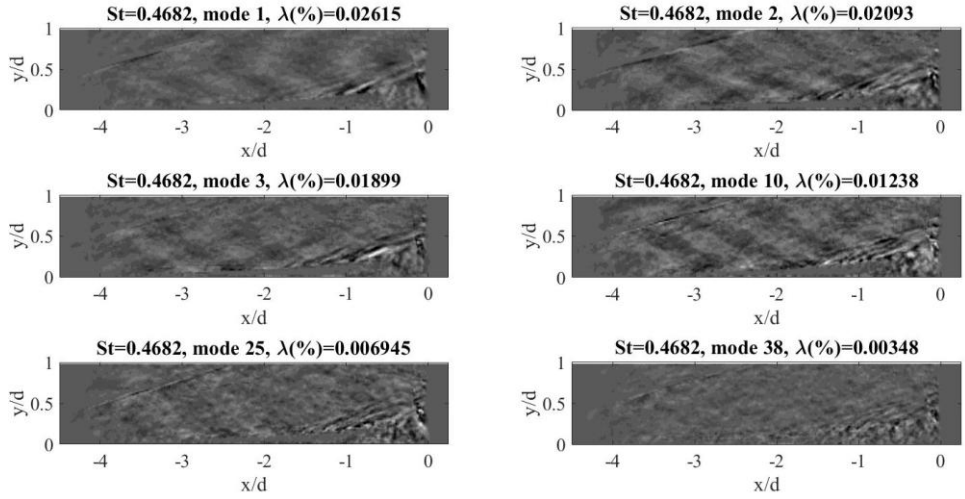

Figure 11. 2-D Plots of Selected Modes at 38.7 kHz

Figure 12 plots the energies of selected modes as a function of Strouhal number. Modes 1, 2, 3, 10, 25, and 38 are examined. As previously stated, low-order modes by definition contain much higher energy levels than higher-order modes and appear to provide better insight into SWBLI unsteadiness. Modes 10 and above have relatively constant modal energies across all Strouhal numbers. Examining Mode 1 however, there is a section between $St = 0.01$ and $St = 0.03$ where energy levels increase before dropping back down again. This jump in energy occurs in the low-frequency range where unsteadiness would be expected. Previous research has found indications of unsteady shock breathing at similar Strouhal numbers, ranging from $St = 0.02 – 0.1$.[4,11,19] Given the results of earlier analysis, the energy jump seen in the current research is likely an indication of shock breathing. Several smaller energy fluctuations are seen in Modes 1 and 2 as Strouhal numbers continue to increase, however these are less significant and occur at higher frequencies and likely do not indicate shock breathing.

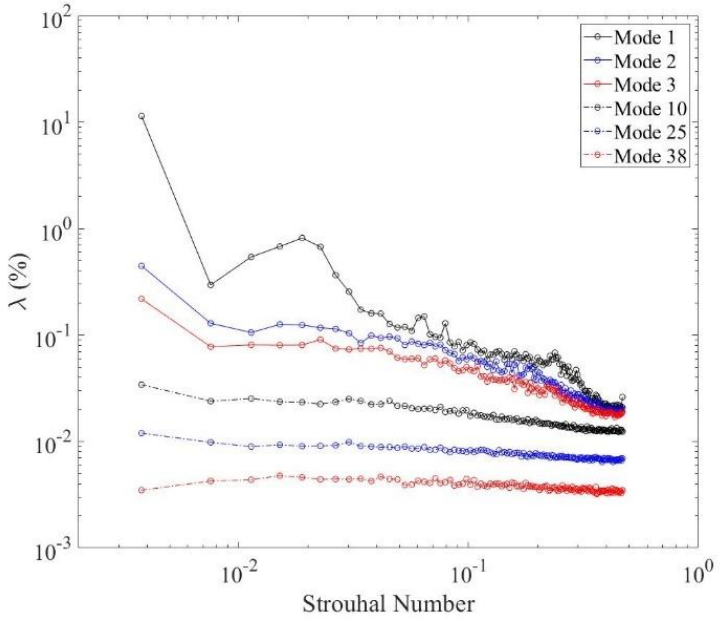

Figure 12.Selected Modal Energies (*λ*) vs. Strouhal Number (*St*)

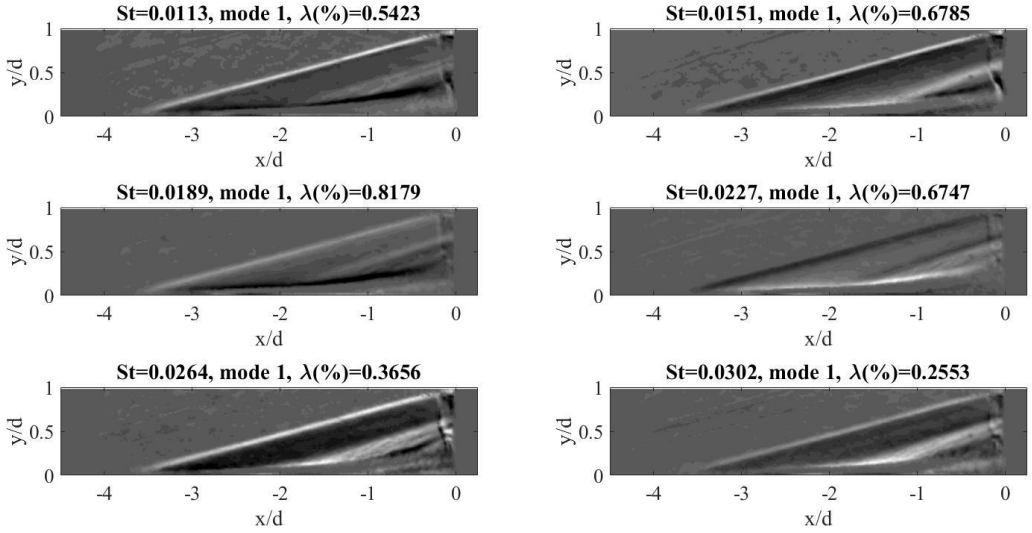

Figure 13. 2-D Plot of Mode 1 for St = 0.01 -0.03

Two-dimensional reconstructions of Mode 1 for *St* = 0.01 – 0.03 are shown in Figure 13. The modal energies peak at λ= 0.8179% for *St* = 0.0189, which corresponds with the plot of Mode 1 in Figure 12. Coherent physical structures form at all six Strouhal numbers examined. The shock structures vary with Strouhal number. Clearly formed *UI*, λ_1, λ_2, and the separation bubble under the lambda-structure are visible for *St* = 0.0113 and *St* = 0.0151. The upstream influence and forward shock lose some definition in the *St* = 0.0189 and *St* = 0.0227 plots, however the boundary layer intensifies as it interacts with λ_1. The separation bubble and λ_2 features become less coherent in the *St* = 0.0264 and *St* = 0.0302 plots as modal energy declines and more turbulence is captured. Examining Figure 12 again, some of the smaller energy jumps previously discussed occur around *St* = 0.06 and *St* = 0.25 for Mode 1. These correspond approximately with Figure 8Figure 10, and comparing the Mode 1 plots for each with those in Figure 13, there is a significant loss in coherence at the larger Strouhal numbers. The structures are much weaker and more turbulence is visible in the separation region and boundary layer. This confirms that these smaller energy jumps do not indicate shock breathing. Additionally, comparing Figure 13 to the Mode 1 plot in Figure 11, which

displays the largest Strouhal number for the data set at $St = 0.4682$, there is an even more significant reduction in the formation of the shock structures. This lack of coherence provides further indication that SWBLI generated unsteadiness does not occur at higher Strouhal numbers.

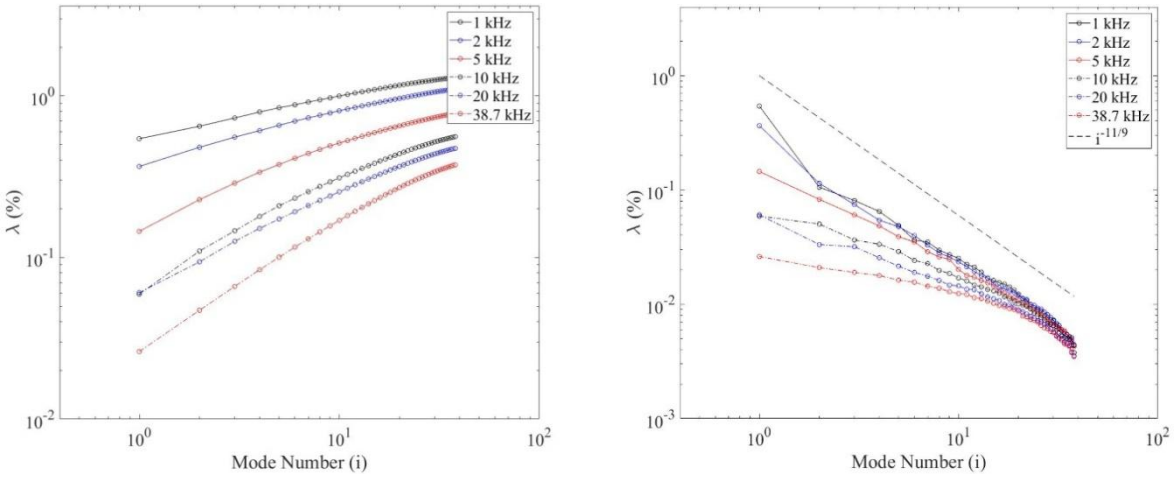

(*a*) (*b*)

Figure 14. Cumulative(*a*) and Per mode (*b*) Energies Plotted vs. Mode Number

Figure 14 (*a*) plots the cumulative percent energies for selected frequencies. The highest percent energies are seen at 1 kHz and 2 kHz, each containing just over 1% of the total energy. The 5 kHz frequency contains around 0.8% of the total energy while frequencies over 10 kHz contain an average of 0.45% of the total energy. Figure 14 (*b*) plots individual energies per mode. Examining the plot, energy levels start off higher for all frequencies and decrease as mode number increases. For this selection, Mode 1 energies range from approximately 0.5% at $f = 1$ kHz to 0.03% at $f = 38.7$ kHz. As mode numbers approach Mode 38, energies for all frequencies converge towards 4×10^{-3} %. These trends are also depicted numerically in Table 1. Figure 14 (*b*) also plots $i^{-11/9}$ as a dashed line, where i is mode number. The linear, downward slope of the line shows an inverse relationship between modal energy and $i^{-11/9}$. This trend has been shown in previous research to be representative of the turbulent energy cascade.[20]

Table 1. Summary of Percent Energy for Selected Modes and Frequencies

Frequency (kHz)	Mode 1	Mode 2	Mode 3	Mode 10	Mode 25	Mode 38
1	0.542	0.106	0.081	0.025	8.9×10^{-3}	4.4×10^{-3}
2	0.366	0.114	0.075	0.024	9.2×10^{-3}	4.4×10^{-3}
5	0.145	0.083	0.061	0.020	8.6×10^{-3}	4.3×10^{-3}
10	0.059	0.050	0.037	0.017	8.1×10^{-3}	3.8×10^{-3}
20	0.061	0.033	0.032	0.015	7.1×10^{-3}	3.5×10^{-3}
38.72	0.026	0.021	0.019	0.012	6.9×10^{-3}	3.5×10^{-3}

Results of the current research show the feasibility of using SPOD for studying SWBLI generated unsteadiness. As demonstrated above, these plots show the resulting structures of the XSWBLIs in a coherent manner, making them key to improving physical understanding of unsteadiness in XSWBLIs. Fine-tuning the parameters within the SPOD algorithm for the current research will optimize SPOD results and allow a more in-depth analysis of modes and frequencies where shock breathing is indicated in the future.

Acknowledgments

This material is based upon research supported by the U. S. Office of Naval Research under award number N00014-15-1-2269. The authors would like to thank Dr. Noel Clemens, Dr. Leon Vanstone, and Dr. Jeremy Jagodzinski for their assistance in the execution of the experiment at UT-Austin as well as Ian Bashor and Eugene

Hoffman for their assistance with test setup, execution, and support. The authors would also like to thank Dr. Jim Coder and Rekesh Ali of UTK who provided assistance with the SPOD code that was the basis of the SPOD script written for the current analysis. The authors also acknowledge Dr. John Schmisseur and Dr. Phillip Kreth at The University of Tennessee Space Institute for their intellectual contributions to the project.

References

[1] Combs, C. S., Lash, E. L., Kreth, P. A., and Schmisseur, J. D., "Investigating Unsteady Dynamics of Cylinder-Induced Shock-Wave/Transitional Boundary-Layer Interactions," *AIAA Journal*, April 2018.

[2] Holden, M. S., "A Review of Aerothermal Problems Associated with Hypersonic Flight," *24th AIAA Aerospace Sciences Meeting and Exhibit*, AIAA Paper 1986-0267, 1986.

[3]Gaitonde, D. V., "Progress in Shock Wave/Boundary Layer Interactions," *Progress in Aerospace Sciences*, Vol. 72, Jan. 2015, pp.80-99.

[4] Clemens, N. T., and Narayanaswamy, V., "Low-Frequency Unsteadiness of Shock Wave/Boundary Layer Interactions," *Annual Review of Fluid Mechanics*, Vol. 46, No. 1, 2014, pp. 469-492.

[5] Murphree, Z. R., Jagodzinski, J., Hood, E. S., Clemens, N. T., and Dolling, D. S., "Experimental Studies of Transitional Boundary Layer Shock Wave Interactions," *44th AIAA Aerospace Sciences Meeting and Exhibit*, AIAA Paper 2006-326, 2006.

[6] Combs, C. S., Kreth, P. A., Schmisseur, J. D., and Lash, E. L., "An Image-Based Analysis of Shock-Wave/Boundary-Layer Interaction Unsteadiness," *AIAA Journal*, Mar. 2018.

[7] Murphree, Z. R., Yuceil, K. b., Clemens, N. T., and Dolling, D. S., "Experimental Studies of Transitional Boundary Layer Shock Wave Interactions," *45th AIAA Aerospace Sciences Meeting and Exhibit*, AIAA Paper 2007-1139, 2007.

[8] Towne, A., Schmidt, O. T., Colonius, T., "Spectral Proper Orthogonal Decomposition and Its Relationship to Dynamic Mode Decomposition and Resolvent Analysis," *Journal of Fluid Mechanics*, May 2018

[9] Welch, P., "The use of fast Fourier transform for the estimation of power spectra: a method based on time averaging over short, modified periodograms," *IEEE Transactions on Audio and Electroacoustics*, Vol. 15-2, pp.70-73

[10] Murphree, Z. R., Combs, C. S., Yu, W. M., Dolling, D. S., Clemens, N. T., "Physics of Unsteady Cylinder-Induced Shock Wave/Transitional Boundary Layer Interactions," *Journal of Fluid Mechanics* (submitted for publication)

[11]Vanstone, L., Seckin,S., and Clemens,N. T. , "POD Analysis of Unsteadiness Mechanisms within a Swept Compression-Ramp Shock-Wave Boundary-Layer Interaction at Mach 2," *AIAA Aerospace Sciences Meeting*,AIAA Paper 2018-2073. 2018.

[12] Hadjadj, A. and J. P. Dussauge, "Shock wave boundary layer interaction," Shock Waves, Vol. 19, No. 6, November, 2009, pp. 449-452.

[13] Dolling, D. S., "Fluctuating Loads in Shock Wave/Turbulent Boundary Layer Interaction: Tutorial and Update," AIAA Paper 93-0284, 31st AIAA Aerospace Sciences Meeting and Exhibit, Reno, NV, January 1993

[14] Knight, D. D. and G. Degrez, "Shock Wave Boundary Layer Interactions in High Mach Number Flows. A Critical Survey of Current Numerical Prediction Capabilities," Advisory Group for Aerospace Research and Development Report No. 319, December, 1998.

[15] Dolling, D.S., N. C. Clemens, and E. Hood, "Exploratory Experimental Study of Transitional Shock Wave Boundary Layer Interactions," Rept. AFRL-SR-AR-TR-03-0046, Jan. 2003.

[16] Dolling, D. S. and S. M. Bogdonoff, "Blunt fin-induced shock wave/turbulent boundary-layer interaction," AIAA Journal, Vol. 20, No. 12, December, 1982, pp. 1674-1680.

[17] Délery, J. and J. G. Marvin, "Shock-Wave Boundary-Layer Interactions," Advisory Group for Aerospace Research and Development Report No. 280, February, 1986

[18] Délery, J. and A. Panaras, "Shock-Wave Boundary-Layer Interactions in High Mach Number Flows," Advisory Group for Aerospace Research and Development Report No. 319, May 1996.

[19] Combs, C. S.,Schmisseur, J. D., Bathel, B.F., and Jones, S.B., "Analysis of Shock-Wave/Boundary-Layer Interaction Experiments at Mach 1.8 and Mach 4.2 Edge Conditions," *AIAA Scitech 2019 Forum*, AIAA Paper 2019.

[20] Mustafa, M.A., Parziale, N.J., Smith, M.S., and Marineau, E.C., "Amplification and Structure of Streamwise-Velocity Fluctuations in Compression-corner Shock-wave/Turbulent Boundary-layer Interactions," *Journal of Fluid Mechanics*, Jan. 2019